

Fabrication of Polymer Membrane-Suspended Microstructures on Printed Circuit Boards

Tanvir Ahmad^{ID}, Student Member, IEEE, Simon Binder^{ID}, Member, IEEE, Moritz Leber^{ID}, Timothy J. Garrett^{ID}, Christopher F. Reiche^{ID}, Member, IEEE, and Florian Solzbacher^{ID}, Fellow, IEEE

Abstract—When microelectromechanical systems are manufactured in high densities, the necessary routing layer structures can become complex and thus expensive if executed in silicon technology. If, additionally, the microstructures are also to be fabricated suspended on membranes, complex thinning processes become necessary to form these often rather fragile membranes. Here, a novel fabrication concept is demonstrated that allows for the fabrication of membrane-suspended microstructures using standard microfabrication techniques directly integrated with printed circuit boards (PCB) by laminating polyimide (PI) films over cavities in the PCB. This results in cost-effective routing layer fabrication and direct compatibility with common electronic component standards such as SMT (surface-mount technology) and THT (through-hole technology). To illustrate the capabilities of the fabrication process, we fabricated an array of membrane suspended microheaters. Individual platinum microheater elements are suspended on PI membranes that are 25 μm thick and 500 μm in diameter. The fabricated PCB carries a 10 × 10 array of suspended microheaters on an area of 26 mm × 26 mm. The characterization of the microheater array shows that a yield of 86% functional microheaters was achieved. An individual microheater shows an almost linear heating characteristic at least up to 200 °C demonstrating the viability of the technique for creating functional membrane-suspended microstructures on a PCB.

[2021-0226]

Index Terms—Microfabrication, membrane-suspended microstructures, MEMS on PCB, polyimide (PI) membrane, microheater array.

I. INTRODUCTION

MICROSTRUCTURES suspended on membranes are essential parts of various microsystems, such as pressure sensors [1]–[3], thermal flow sensors [4]–[6], gas sensors [7], [8], audio frequency filters [9], optical filters [10], microactuators [11], [12] and infrared emitters [13]. Depending on the application, these thin membranes serve different

Manuscript received October 18, 2021; revised March 6, 2022; accepted March 8, 2022. Date of publication April 8, 2022; date of current version June 2, 2022. This work was supported by the United States Department of Energy under Award DE-SC0017168 (awarded to Particle Flux Analytics Inc.). The work of Simon Binder was supported by the Deutsche Forschungsgemeinschaft (German Research Foundation, DFG) under Project 459675326. Subject Editor D. DeVoe. (Corresponding author: Christopher F. Reiche.)

Tanvir Ahmad, Simon Binder, Moritz Leber, Christopher F. Reiche, and Florian Solzbacher are with the Department of Electrical and Computer Engineering, The University of Utah, Salt Lake City, UT 84112 USA (e-mail: christopher.reiche@utah.edu).

Timothy J. Garrett is with the Department of Atmospheric Sciences, The University of Utah, Salt Lake City, UT 84112 USA.

Color versions of one or more figures in this article are available at <https://doi.org/10.1109/JMEMS.2022.3162785>.

Digital Object Identifier 10.1109/JMEMS.2022.3162785

purposes, ranging from thermal isolation of components to improving sensor performance parameters such as sensitivity, response time and low power consumption as well as high positioning accuracy of moveable structures. These thin membranes can be fabricated from various materials, such as silicon [14], silicon dioxide [15], [16], silicon nitride [17], [18], silicon carbide [19] or a variety of polymers [20]. In particular, the polymer polyimide (PI) has been used as a membrane material in several works to suspend microstructures such as microheaters, using either silicon-based substrates [21], [22] or even without a solid substrate [23]. Polymers allow membrane-suspended structures to be also implemented on non-silicon-based substrates. One of the most common wiring carriers for electric components are printed circuit boards (PCB). With their high component compatibility, multilayer technology for advanced routing and low-cost production, they offer many advantages, which is why they appear very attractive as a carrier board for microelectromechanical structures. The direct fabrication of MEMS devices with PCB technology has been the subject of research for some time [24]–[26]. Such devices are often referred to as PCB-MEMS [27]. Among the numerous PCB-MEMS devices presented in the past, there are also devices with membrane-suspended structures in particular such where a PI layer is used as the membrane material. A structured PI layer, which carries copper electrodes, is, e.g., used in an RF-MEMS capacitive switch [28]. In another application, a PI membrane is used to suspend a mass in a microelectromechanical accelerometer [10], [29].

In this work we present a novel fabrication technique to fabricate PI membrane-suspended microstructures with standard microfabrication techniques directly on PCBs to integrate both technologies. Using a PCB as a substrate the PCB's multilayer technology becomes available for cost-effective advanced routing options as they are needed to wire a high density heater array properly. In addition, the many advantages of PCBs as a wiring carrier become available, such as low manufacturing costs, expanded integration properties with PCB-compatible components and rapid prototyping capabilities. Furthermore, we show the exemplary fabrication and characterization of a 10 × 10 array of PI membrane-suspended microheaters on a PCB with vias for routing purposes. Microheaters were chosen as the demonstration device for this new fabrication method, because of their many applications, such as in mass flow meters [30], gas sensors [31], infrared emitters [13], fuel cells [36], fingerprint sensors [37] or weather sensors

[38], [39]. Additionally, their fabrication requires many standard fabrication processes such as physical vapor deposition, wet- and dry etching as well as photolithography.

For the operation of microheaters it is favorable if they are made on thinned materials with low thermal conductivity to, e.g., reach low power consumption [32], [33] as the thin low thermal conductivity layer reduces heat dissipation to the substrate. PI is a flexible PCB substrate material that has been used for this purpose in the past for microheaters in applications such as thermal gas flow meters [34].

In the structures described in this work, a standard PCB is used that contains drill holes that act as cavities and a PI film laminated on the PCB fulfills the function of the thin membrane and substrate on which the platinum microheaters are created. Membrane-forming thinning processes that are often necessary in silicon-based membrane-suspended microheater structures are thus avoided and being replaced by a simple lamination of the PI film onto the PCB [35].

II. DEVICE FABRICATION

The fabrication of the membrane-suspended microstructures can be divided into four major steps. In the first step, a PI layer is laminated onto the PCB so that the membrane is formed over the PCB's cavities (Section II-B). Then, in a second step, the PI is removed locally in the area over the copper vias or contact pads on the PCB by dry etching so that these are accessible for subsequent wiring (Section II-C). In a third step, the desired microstructure is created using the PI layer as a substrate. In the case of the demonstrated microheater array, meander-shaped platinum microheaters are deposited on the membranes, including platinum conducting tracks to the openings of the PI layer (Section II-D). In a fourth step, the electrical contact between the microstructures and the PCB's exposed copper vias/contact pads is enhanced by filling the space above the copper vias/contact pads with aluminum or another metal. As an optional step, another PI layer can be laminated over the entire microstructured area to protect it from environmental influences (Section II-E).

A. Layout of the Microstructure Elements and PCB

Before the microstructures can be fabricated, their layout, as well as that of the corresponding PCB, need to be designed. While this depends on the type of microstructure to be fabricated, it is important to include alignment marks in both layouts to enable the alignment of the microstructure layer to the PCB's vias/contact pads. In the microstructure design there should be contact pads included that are in the same position but slightly larger than the corresponding vias/contact pads on the PCB to ensure a reliable electrical connection during device fabrication.

Fig. 1 a shows the layout of a single heater element used for the demonstration device. A commercially available PI film (Kapton 150FN019, Dupont) with thickness of 25.4 μm is chosen as the membrane material. A platinum meander forms the microheater with dimensions as shown. The thickness of the Pt thin film is 110 nm and the assumed sheet resistance is 0.2 Ω_{sq} resulting in an overall targeted resistance of the

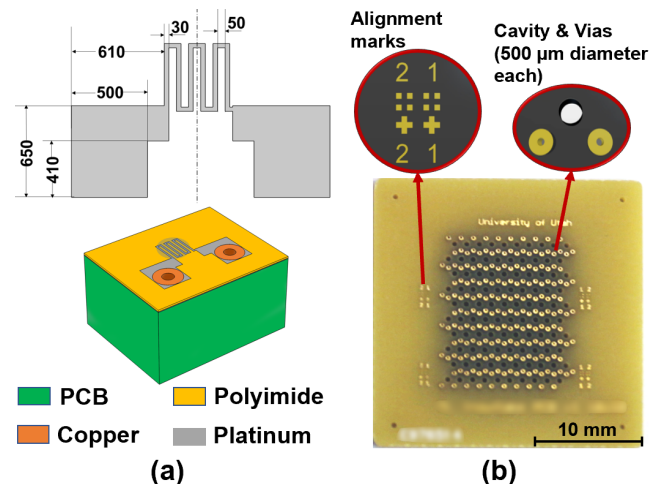


Fig. 1. (a) Dimensions of a single platinum microheater element in μm and (b) layout of the PCB for a 10×10 microheater array.

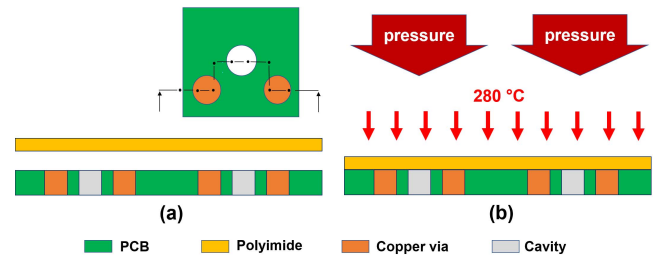


Fig. 2. (a) Attaching the PI film to the PCB using the adhesive and (b) heat press lamination process by applying a temperature of 280 $^{\circ}\text{C}$.

structure of 200 Ω . The layout of the corresponding 2-layer PCB board (26 mm \times 26 mm \times 1.2 mm) is shown in Fig. 1 b. It contains 100 cavities of 500 μm diameter each arranged in a 10×10 array. For each cavity there are two corresponding copper vias to route the heaters' electrical connections to the back of the PCB. The chosen PCB material is based on FR-4 and the boards were ordered from a commercial supplier (Eurocircuits).

B. Membrane Formation

In this first step, the membranes are formed. The cavities consist of drill holes (or other hole-like structures) in the PCB material. The PI film used has an adhesive layer of fluorinated ethylene propylene (Kapton 150FN019, 25.4 μm thickness with 12.7 μm thick adhesive layer, Dupont). Using the adhesive side facing the PCB, the PI film is attached on top of latter (Fig. 2). The lamination process is completed by utilizing a heat press (Geo Knight JP 12) at 280 $^{\circ}\text{C}$ for 90 s. The membrane results from the lamination of the PI film over the PCB's cavities. The laminated samples are cleaned with Acetone, followed by Isopropyl alcohol (IPA) and DI water. Subsequently, the PI laminated PCB sample is mounted on a wafer using double-sided Kapton tape to ensure micro fabrication equipment compatibility. Fig. 3 shows the result of this first fabrication step.

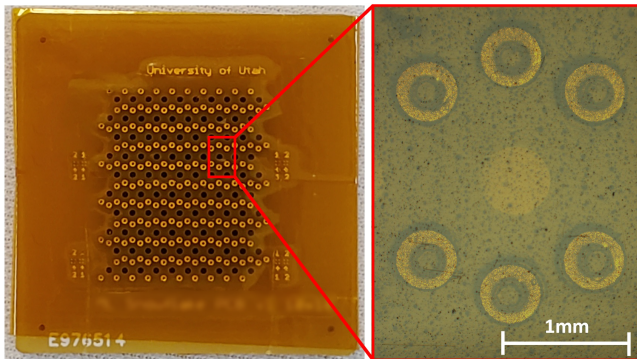


Fig. 3. Image of the PCB after the lamination step with a closeup on the PI covered copper vias and cavity.

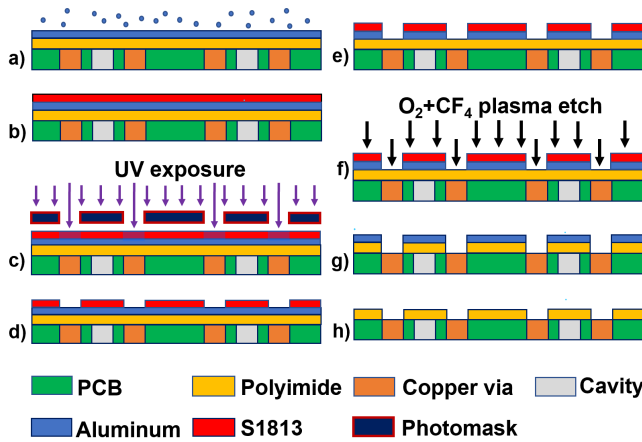


Fig. 4. Process steps for via/contact pad PI film opening: (a) aluminum deposition, (b) to (d) spin-coating, exposure and development, (e) wet etching of the aluminum (f) dry etching of the PI and (g) to (h) stripping of the aluminum hard mask.

C. Via/Contact Pad PI Film Opening

After the lamination of the PI film onto the PCB the vias (or contact pads, depending on PCB design) are covered by the PI. Thus, the PI needs to be removed locally to expose the vias/contact pads in order to form electrical connections. The corresponding patterning process that uses an aluminum hard mask to locally dry etch the PI is illustrated in Fig. 4. First, a 700 nm layer of aluminum is deposited on the PI in a vacuum sputtering process (Denton Discovery 18, Argon gas flow: 50 sccm, Sputter power: 100 W). The sample is spin-coated with a positive photoresist (S1813, CEE 200X Spinner, Spin speed: 2000 rpm, Spin time: 45 s), softbaked (110°C for 2 min, Binder FD 53-UL oven) and subsequently UV-exposed through a photo mask (Suss MA1006, Wavelength: 365 nm, Dose: 60 $\frac{\text{mJ}}{\text{cm}^2}$). The exposed sample is then developed (45 s, AZ1:1 developer solution) and rinsed with DI water afterwards. The aluminum layer is selectively etched by wet etching (aluminum etchant type A) to create the dry etching windows and rinsed with DI water afterwards. The PI is then dry etched by reactive ion etching using a CF₄/O₂ 10:50 plasma (Oxford ICP 100, Forward power: 1000 W, RF power: 300 W, RF bias: 190 V, Chuck temperature: -10°C, Etch time: 50 min). Sealing the edges of the PCB with Kapton tape (Tape 5413, 3 M) ensures that no etchant

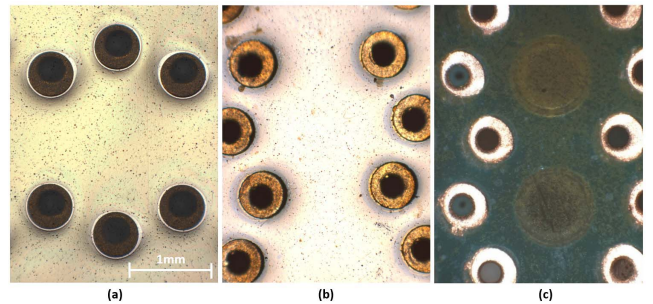


Fig. 5. Image of (a) the PI layer covered by the aluminum hard mask, (b) the locally dry etched PI in the via area and (c) the PCB after the removal of the aluminum hard mask.

invades beneath the PCB damaging the covered membrane from below. Afterwards, the dry etched sample is dipped in an HF bath for 15 s to remove residue created during the dry etching step. Finally, the remaining aluminum is stripped off by wet etching as described above and rinsed with DI water afterwards. Images of the interim states as well as the final result of this subsection's process are shown in Fig. 5.

D. Microstructure Formation

In this step, the required microstructure is formed on top of the PI film. Please note, that the process depends on the type of the microstructure that one aims to create and thus needs to be designed accordingly. Here, a process that can be used to form Pt microheaters is described and is illustrated in Fig. 6. First, the sample is spin-coated with positive photoresist (AZ9260, CEE 200X Spinner, spin speed: 1000 rpm, spin time: 1 min) and subsequently soft baked (10 min at 110°C, Binder UL51 oven) and rehydrated overnight by leaving the substrates in a closed chamber which contains a large surface water tray to ensure high humidity. Afterwards, the sample is UV exposed through a dark field mask (Suss MA1006, Wavelength: 365 nm, Dose: 220 $\frac{\text{mJ}}{\text{cm}^2}$). In the present case, the exposure was divided in three steps, with 10 seconds pause in between. The exposed sample is developed (AZ400K solution for 8 min) and rinsed with DI water afterwards. After development, the PI surface of the sample is O₂ plasma treated for 1 min in a planar plasma etcher (Technics PE IIA, power: 100 W, flow: 51.1 sccm, pressure: 280 mTorr) to improve metal adhesion. In the next step, first a 5 nm adhesion layer of titanium is sputter deposited (Denton Discovery 18, Power: 50 W) followed by a 110 nm layer of platinum (Denton Discovery 18, Power: 50 W). The microheater structures are patterned by a lift-off process in an ultrasonicated Acetone bath (30 min) followed by rinsing with IPA and DI water. Fig. 7 shows an image of the deposited heater layer as a result of this process substep.

E. Via/Contact Pad Contacting and Encapsulation

The microstructures that were created in the previous step should include a routing layer with the contact pads deposited over the opened holes in the PI film. This usually thin material layer already connects the microstructure layer on the PI film substrate to the PCB's vias/contact pads due to sputtering under an angle of approx. 150° instead of 180° between

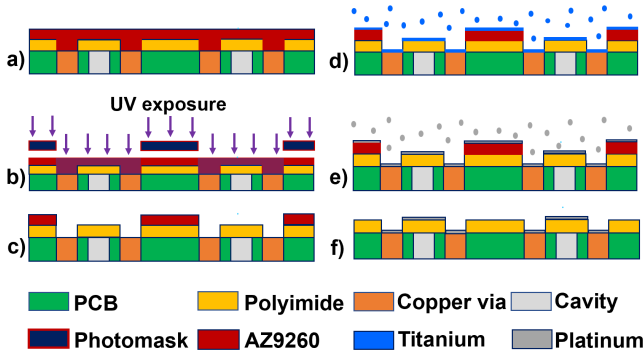


Fig. 6. Microheater patterning steps: (a) to (c) Spin-coating AZ9260, exposure and development, (d) titanium deposition, (e) platinum deposition and (f) platinum lift-off.

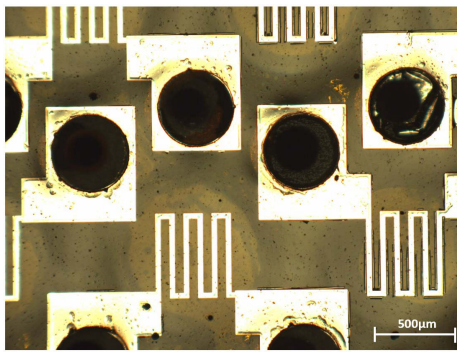


Fig. 7. Image of the platinum heater structures, which are deposited onto the PI membranes.

the PCB substrate surface and the sputtering target surface. However, it was found that the resulting electrical connection is unreliable. Therefore, to reinforce the electrical connection between the contact pads on the microstructure layer and the vias/contact pads on the PCB, an additional layer of aluminum is deposited on the corresponding area to reinforce and ensure the electrical connection (see Fig. 8). For this purpose, the sample is first coated with a positive photoresist (AZ9260, CEE 200X Spinner, spin speed: 1000 rpm, spin time: 1 min), soft baked (10 min at 110 °C, Binder UL51 oven), rehydrated overnight, subsequently UV exposed through another photo mask (Suss MA1006, Wavelength: 365 nm, Dose: 220 $\frac{\text{mJ}}{\text{cm}^2}$, 3-step exposure with 10 s pause in between) and developed with AZ400K solution for 8 min. Afterwards the sample is rinsed with DI water and O₂ plasma treated (Technics PE IIA, power: 100 W, flow: 51.1 sccm, pressure: 280 mTorr, time: 1 min). Then, a 700 nm thick layer of aluminum is sputter deposited (Denton Discovery 18, Argon gas flow: 50 sccm, Sputter power: 100 W). The aluminum contact pads are subsequently patterned via a lift-off process by placing the samples in an ultrasonic Acetone bath for 30 min followed by rinsing with IPA and DI water. The result of this substep is shown in Fig. 9 and gives an impression of the aluminum deposition area. Finally, as an optional step, the microstructures and openings in the PI film can be encapsulated to protect them from the environment. This can be achieved by laminating the sample with another layer of PI as described in Section II-B.

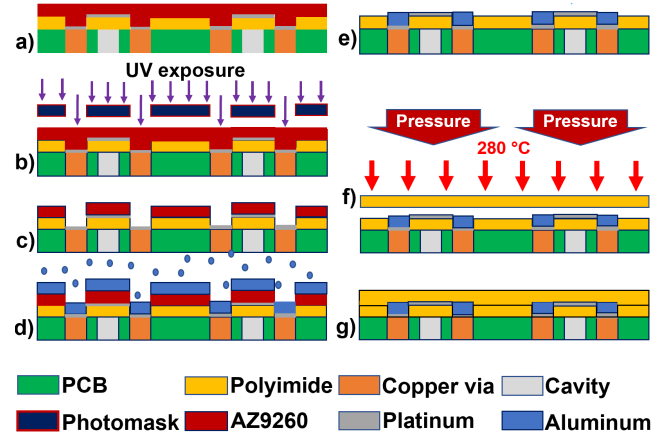


Fig. 8. Via contacting and encapsulation process: (a) to (c) spin-coating, exposure and development, (d) aluminum sputter deposition, (e) aluminum lift-off and (f) to (g) PI encapsulation.

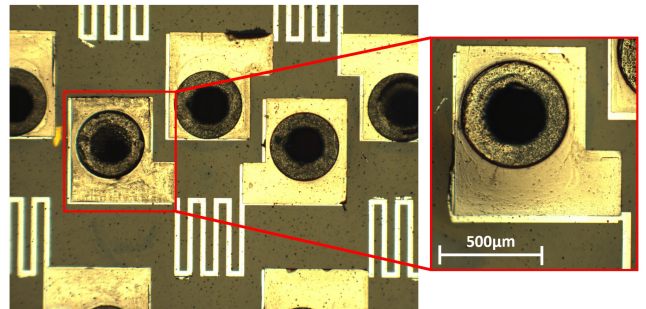


Fig. 9. Image of the substrate after aluminum deposition with a closeup of a single via/contact pad. The aluminum is deposited in the area of the PCB's copper via and the PI's contact pad area.

F. Microstructure Characterization and Testing

After completing the fabrication of the devices, they can be characterized and tested. In the case of the microheater arrays, six devices each containing a 10 × 10 microheater array were fabricated (see Fig. 10). Please note that the optional encapsulation step was not performed for these measurements. Only after completion of all the described characterizations, this optional encapsulation was added.

First, the resistance of each microheater was measured by contacting the vias from the backside with a digital multimeter. To characterize the heating behaviour of an individual microheater it was powered with a DC power supply. The power input was gradually increased. The temperature and the thermal distribution of the heater was observed with a thermal camera (FLIR T420) coupled with a 2X zoom lens at an ambient temperature of 20 °C. For these measurements the camera was set to an emissivity of 0.9.

III. RESULTS AND DISCUSSION

Out of the 600 fabricated microheaters, 518 were found to be working, thus giving a yield of 86.3%. Failed devices are due to short-circuits (1.2%) and open-loop configuration (12.5%). The microheater structures were visually inspected with an optical microscope (Keyence VHX-5000). Fig. 11

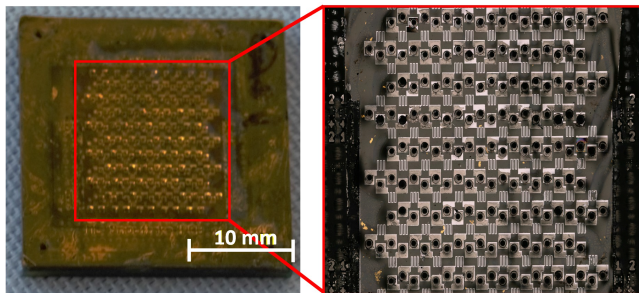


Fig. 10. Final PCB device and close-up of the 10×10 microheater array.

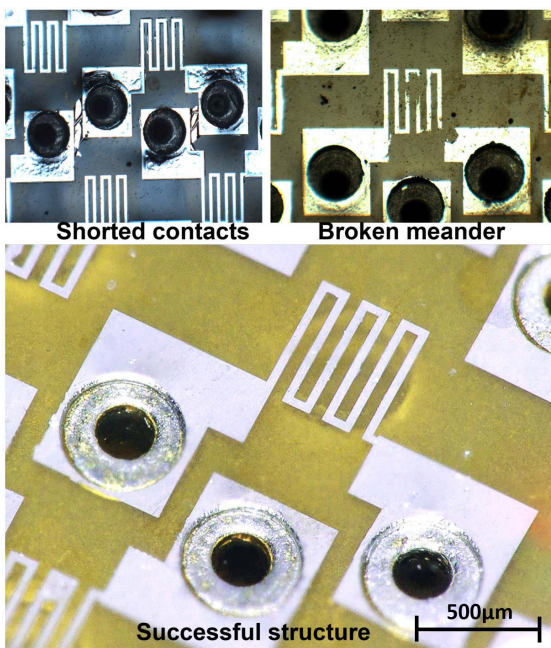


Fig. 11. Close up image of a membrane-suspended microheater with examples of failed microheaters.

shows the close-up image of a successfully fabricated microheater (image taken before encapsulation step) as well as examples of failed heaters, i.e. a microheater with shorted contacts and broken structures due to unsuccessful lift-off. The average resistance of a microheater is 251.2Ω . Fig 12 shows the distribution of all working microheaters' resistance values from the in total six microheater arrays fabricated. The targeted resistance for each microheater from the preliminary design calculation was 200Ω . Fig. 13 gives an exemplary graphical representation of resistance values as well as the type of failure depending on the position of the microheaters for one of the six fabricated heater arrays. While the results of this exemplary fabrication run can be certainly improved, with respect to homogeneity of the resistances and yield with further process improvements, for example by using a two layer lift-off photoresist, this nonetheless shows the feasibility of this novel fabrication method to create viable microstructures and devices. Due to the lower stiffness of PI compared to standard microfabrication membrane materials such as silicon nitride, the PI membrane may exhibit a small deformation when suspended over a larger hole. This could lead to device

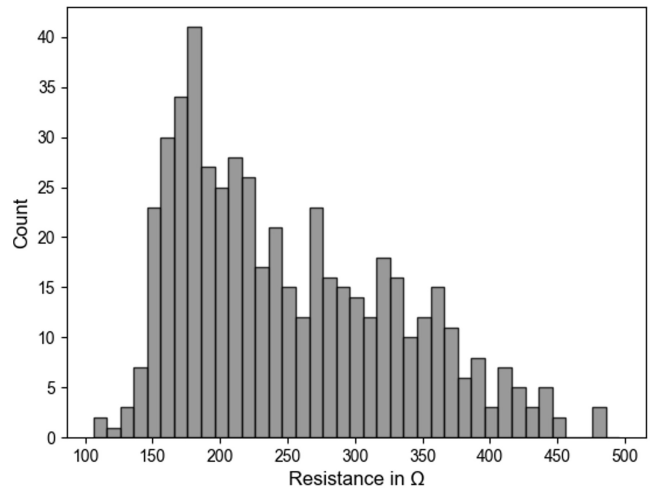


Fig. 12. Histogram of the total resistance values from the six fabricated microheater arrays.

	1	2	3	4	5	6	7	8	9	10
1	370	333	450		364	411			370	
2	280	320	218	401	332	320	380	390		330
3	275	227	340	480	350	343	357	322	325	250
4	198	305	305	264	330	332	350	360		265
5	293	241	292	272	305	370		330		252
6	305		214	253	218	185	360	312	292	268
7	204	245	223		162	340	388	300	280	270
8	172	190	206	160	223	224	220		275	260
9	172	170	176	204	285	240	285	300	336	273
10	167	145	168	182		178	278	266	226	216

Shorted structures **Resistance > 1000 Ω**

140 Ω 200 Ω **500 Ω**

Fig. 13. Exemplary resistance values (in Ω) as well as failure types of one of the six microheater arrays manufactured to show the spatial distribution (the numbers on white background correspond to the array index of the heaters on the device).

failure due to the surface being curved with potential failure points at the membrane's edge or more challenging photolithography steps. Depending on the microstructure to be suspended this behaviour of the PI membrane needs to be considered in the design process. In the present exemplary case of the microheaters, the smaller stiffness of the PI did not pose a severe issue as can be seen from the high rate of functional devices.

Fig. 14 a shows the thermal image of a microheater operating at 100°C . The heat is localized in the meander over the cavity area and the temperature of the contact pads are close to the ambient temperature. Fig. 14 b shows the temperature at the center of the microheater as a function of the applied input power. The heater's thermal response was found to be linear in the tested temperature range. The examined fabricated microheater consumed approx. 32.3 mW to reach 100°C at room temperature environment. In an experiment it was found that the microheater was able to

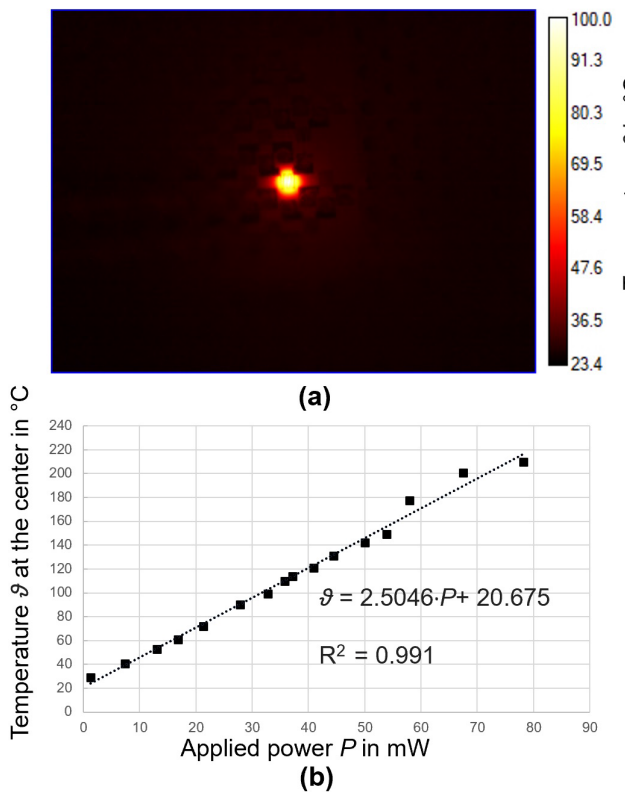


Fig. 14. (a) Thermal image of a single microheater operating at 100°C and (b) temperature at the center of a microheater as a function of the input power. The dotted line indicates a linear fit with the fit parameters given. Please note that for all measurements the final optional lamination step was not performed on the samples. Therefore, the heaters were not covered by a PI film.

heat up to 450°C consuming 220 mW power. For temperatures above 450°C, the heater failed to function. This could have several reasons: first, the data sheet of the Kapton PI film which was used as a membrane for the devices states that the PI is subject to oxidative degradation. This oxidative degradation is temperature dependent and limits the lifetime of the PI at temperatures above 400°C drastically (down to a few hours or less) [21], [40], [41]. Second, the current density in the platinum meander observed at this maximum temperature is approx. $1 \times 10^6 \text{ A cm}^{-2}$ and is thus in the range of maximum current densities achieved in previous works [17]. Therefore, two possible failure modes exist: on the one hand the membrane could be destroyed by oxidative degradation at temperatures above 400°C. On the other hand, it is also possible that the heater structure exceeded its maximum current density limitations at roughly the same temperature. While the dimensions and geometry of the platinum meander may be changed to allow higher current densities, the membrane material remains a limiting factor due to the oxidative degradation. This points to the membrane material as limiting factor for the maximum temperature that can be reached with heater structures fabricated with this method.

IV. CONCLUSIONS

In this publication a new fabrication method for polymer-based membrane-suspended microstructures directly integrated with standard PCBs was introduced. By using PCBs as substrates, cost-effective PCB multilayer routing for high packing densities of microstructures can be employed.

Additionally, due to the PCB-based approach, direct connectivity to other standard electronic components can be achieved without additional bonding processes.

The process was exemplified on an example process fabricating an array of microheaters while using a PI membrane on top of a 2-layer PCB. The fabricated 10 × 10 microheater array covers an area of 26 mm × 26 mm. These devices demonstrate the feasibility of the method with a yield of 86% and a linear power to heat transfer behaviour in a temperature range between room temperature and up to at least 200°C.

Besides further optimization of the fabrication process to increase the yield it could be even further simplified by replacing the aluminum hard mask and dry etching-based patterning with laser ablation. By eliminating the aluminum hard mask from the process flow the fabrication would be drastically simplified. This option will be explored in future research.

The demonstrated microheater array itself could potentially be used for common microheater applications, like e.g. gas sensors or hot film anemometers, in the future. Furthermore, the presented technique also allows for the fabrication and rapid-prototyping of other membrane-suspended microstructures, e.g. pressure sensors, filters or microactuators, harnessing PCBs as a low-cost routing solution.

ACKNOWLEDGMENT

The authors would like to thank Allan Reaburn and his colleagues at Particle Flux Analytics for their key contributions in the development of devices based on the described fabrication technique. Eric Pardyjak for providing the FLIR T420 thermal camera for the experiments and Brian Baker for further helpful discussions are also gratefully acknowledged. This work was performed in part at the Utah Nanofab which is sponsored by the University of Utah's College of Engineering, Office of the Vice President for Research, and the Utah Science Technology and Research (USTAR) initiative of the State of Utah. The authors appreciate the support of the staff and facilities that made this work possible.

The authors declare the following potentially competing financial interests that are managed through the University of Utah conflict of interest management: Florian Solzbacher declares a financial interest in Sentiomed, Inc. and Blackrock Microsystems/Blackrock Neuromed. Timothy J. Garrett is a co-owner of Particle Flux Analytics Inc., which manufactures and sells a device based on the described fabrication technique. The fundamental intellectual property of the presented fabrication process is protected by the following patent application filed by the University of Utah Research Foundation, exclusively licensed to and commercially available through Particle Flux Analytics, Inc.: Micro-Electromechanical Systems Including Printed Circuit Boards and Pre-Fabricated Polymer Films, WO 2020061356A2 with Moritz Leber, Florian Solzbacher, and Brian Baker listed as inventors.

REFERENCES

- [1] A. Kuoni, R. L. Holzherr, M. Boillat, and N. F. D. Rooij, "Polyimide membrane with ZnO piezoelectric thin film pressure transducers as a differential pressure liquid flow sensor," *J. Micromech. Microeng.*, vol. 13, no. 4, pp. S103–S107, Jul. 2003, doi: [10.1088/0960-1317/13/4/317](https://doi.org/10.1088/0960-1317/13/4/317).

- [2] S.-C. Gong, "Effects of pressure sensor dimensions on process window of membrane thickness," *Sens. Actuators A, Phys.*, vol. 112, nos. 2–3, pp. 286–290, May 2004, doi: [10.1016/j.sna.2004.02.001](https://doi.org/10.1016/j.sna.2004.02.001).
- [3] W. Hasenkamp *et al.*, "Polyimide/SU-8 catheter-tip MEMS gauge pressure sensor," *Biomed. Microdevices*, vol. 14, no. 5, pp. 819–828, Oct. 2012, doi: [10.1007/s10544-012-9661-8](https://doi.org/10.1007/s10544-012-9661-8).
- [4] E. Yoon and K. D. Wise, "An integrated mass flow sensor with on-chip CMOS interface circuitry," *IEEE Trans. Electron Devices*, vol. 39, no. 6, pp. 1376–1386, Jun. 1992, doi: [10.1109/16.137317](https://doi.org/10.1109/16.137317).
- [5] B. Yu, Z. Gan, S. Cao, J. Xu, and S. Liu, "A micro channel integrated gas flow sensor for high sensitivity," in *Proc. 11th Intersoc. Conf. Thermal Thermomech. Phenomena Electron. Syst.*, May 2008, pp. 215–220, doi: [10.1109/ITHERM.2008.4544273](https://doi.org/10.1109/ITHERM.2008.4544273).
- [6] N. Sabaté, J. Santander, L. Fonseca, I. Gràcia, and C. Cané, "Multi-range silicon micromachined flow sensor," *Sens. Actuators A, Phys.*, vol. 110, nos. 1–3, pp. 282–288, Feb. 2004, doi: [10.1016/j.sna.2003.10.068](https://doi.org/10.1016/j.sna.2003.10.068).
- [7] I. Simon and M. Arndt, "Thermal and gas-sensing properties of a micromachined thermal conductivity sensor for the detection of hydrogen in automotive applications," *Sens. Actuators A, Phys.*, vols. 97–98, pp. 104–108, Apr. 2002, doi: [10.1016/S0924-4247\(01\)00825-1](https://doi.org/10.1016/S0924-4247(01)00825-1).
- [8] S. Roy, C. K. Sarkar, and P. Bhattacharyya, "Ultrasensitive Pd-Ag/ZnO/nickel alloy-based metal-insulator-metal methane sensor on micromachined silicon substrate," *IEEE Sensors J.*, vol. 12, no. 7, pp. 2526–2527, Jul. 2012, doi: [10.1109/JSEN.2012.2195166](https://doi.org/10.1109/JSEN.2012.2195166).
- [9] K.-N. Lee, D.-S. Lee, S.-W. Jung, Y.-H. Jang, Y.-K. Kim, and W.-K. Seong, "A high-temperature MEMS heater using suspended silicon structures," *J. Micromech. Microeng.*, vol. 19, no. 11, Nov. 2009, Art. no. 115011, doi: [10.1088/0960-1317/19/11/115011](https://doi.org/10.1088/0960-1317/19/11/115011).
- [10] D. Hohlfeld, M. Epmeier, and H. Zappe, "A thermally tunable, silicon-based optical filter," *Sens. Actuators A, Phys.*, vol. 103, nos. 1–2, pp. 93–99, 2003, doi: [10.1016/S0924-4247\(02\)00320-5](https://doi.org/10.1016/S0924-4247(02)00320-5).
- [11] M. Khoo and C. Liu, "Micro magnetic silicone elastomer membrane actuator," *Sens. Actuators A, Phys.*, vol. 89, no. 3, pp. 259–266, 2001, doi: [10.1016/S0924-4247\(00\)00559-8](https://doi.org/10.1016/S0924-4247(00)00559-8).
- [12] N. A. Hamid, B. Y. Majlis, J. Yunas, A. R. Syafeeza, Y. C. Wong, and M. Ibrahim, "A stack bonded thermo-pneumatic micro-pump utilizing polyimide based actuator membrane for biomedical applications," *Microsyst. Technol.*, vol. 23, no. 9, pp. 4037–4043, Sep. 2017, doi: [10.1007/s00542-016-2951-y](https://doi.org/10.1007/s00542-016-2951-y).
- [13] K.-H. Lee, H.-K. Lee, H.-J. Byun, I.-J. Cho, J.-U. Bu, and E. Yoon, "An audio frequency filter application of micromachined thermally-isolated diaphragm structures," *Sens. Actuators A, Phys.*, vol. 89, nos. 1–2, pp. 49–55, 2001, doi: [10.1016/S0924-4247\(00\)00539-2](https://doi.org/10.1016/S0924-4247(00)00539-2).
- [14] S. Roy, C. K. Sarkar, and P. Bhattacharyya, "A highly sensitive methane sensor with nickel alloy microheater on micromachined Si substrate," *Solid-State Electron.*, vol. 76, pp. 84–90, Oct. 2012, doi: [10.1016/j.sse.2012.05.040](https://doi.org/10.1016/j.sse.2012.05.040).
- [15] D. Barrettillo, M. Graf, S. Taschini, S. Hafizovic, C. Hagleitner, and A. Hierlemann, "CMOS monolithic metal–oxide gas sensor microsystems," *IEEE Sensors J.*, vol. 6, no. 2, pp. 276–286, Apr. 2006, doi: [10.1109/JSEN.2006.870156](https://doi.org/10.1109/JSEN.2006.870156).
- [16] A. Götz *et al.*, "A micromachined solid state integrated gas sensor for the detection of aromatic hydrocarbons," *Sens. Actuators, B, Chem.*, vol. 44, nos. 1–3, pp. 483–487, 1997, doi: [10.1016/S0925-4005\(97\)00171-8](https://doi.org/10.1016/S0925-4005(97)00171-8).
- [17] J. Courbat, D. Briand, and N. F. de Rooij, "Reliability improvement of suspended platinum-based micro-heating elements," *Sens. Actuators A, Phys.*, vol. 142, no. 1, pp. 284–291, Mar. 2008, doi: [10.1016/j.sna.2007.04.006](https://doi.org/10.1016/j.sna.2007.04.006).
- [18] Y. W. Lai and J. E.-Y. Lee, "In situ study of thermal deformation of metal resistive heater on silicon nitride membrane by digital holographic microscopy," in *Proc. 7th IEEE Int. Conf. Nano/Micro Eng. Mol. Syst. (NEMS)*, Mar. 2012, pp. 557–561, doi: [10.1109/NEMS.2012.6196837](https://doi.org/10.1109/NEMS.2012.6196837).
- [19] P. M. Sarro, "Silicon carbide as a new MEMS technology," *Sens. Actuators A, Phys.*, vol. 82, nos. 1–3, pp. 210–218, 2000, doi: [10.1016/S0924-4247\(99\)00335-0](https://doi.org/10.1016/S0924-4247(99)00335-0).
- [20] A. G. P. Kottapalli, M. Asadnia, J. M. Miao, G. Barbastathis, and M. S. Triantafyllou, "A flexible liquid crystal polymer MEMS pressure sensor array for fish-like underwater sensing," *Smart Mater. Struct.*, vol. 21, no. 11, 2012, Art. no. 115030, doi: [10.1088/0964-1726/21/11/115030](https://doi.org/10.1088/0964-1726/21/11/115030).
- [21] M. Aslam, C. Gregory, and J. V. Hatfield, "Polyimide membrane for micro-heated gas sensor array," *Sens. Actuators B, Chem.*, vol. 103, nos. 1–2, pp. 153–157, Sep. 2004, doi: [10.1016/j.snb.2004.04.102](https://doi.org/10.1016/j.snb.2004.04.102).
- [22] D. Briand *et al.*, "Micro-hotplates on polyimide for sensors and actuators," *Sens. Actuators A, Phys.*, vol. 132, no. 1, pp. 317–324, 2006, doi: [10.1016/j.sna.2006.06.003](https://doi.org/10.1016/j.sna.2006.06.003).
- [23] J. Courbat, M. Canonica, D. Teyssieux, D. Briand, and N. F. de Rooij, "Design and fabrication of micro-hotplates made on a polyimide foil: Electrothermal simulation and characterization to achieve power consumption in the low mW range," *J. Micromech. Microeng.*, vol. 21, no. 1, Jan. 2011, Art. no. 015014, doi: [10.1088/0960-1317/21/1/015014](https://doi.org/10.1088/0960-1317/21/1/015014).
- [24] T. Merkel, M. Graeber, and L. Pagel, "A new technology for fluidic microsystems based on PCB technology," *Sens. Actuators A, Phys.*, vol. 77, no. 2, pp. 98–105, 1999, doi: [10.1016/S0924-4247\(99\)00062-X](https://doi.org/10.1016/S0924-4247(99)00062-X).
- [25] D. Fries *et al.*, "PCB MEMS for environmental sensing systems," in *Proc. 31st Annu. Conf. IEEE Ind. Electron. Soc. (IECON)*, 2005, p. 5, doi: [10.1109/IECON.2005.1569271](https://doi.org/10.1109/IECON.2005.1569271).
- [26] A. Luque, J. M. Soto, F. Perdigones, C. Aracil, and J. M. Quero, "Electroosmotic impulsion device for integration in PCB-MEMS" in *Proc. Spanish Conf. Electron. Devices*, Feb. 2013, pp. 119–122, doi: [10.1109/CDE.2013.6481357](https://doi.org/10.1109/CDE.2013.6481357).
- [27] R. Ramadoss, A. Luque, and C. Aracil, "PCB based MEMS and microfluidics," in *MEMS Packaging* (WSPC Series in Advanced Integration and Packaging). 2018, ch. 6, pp. 85–115, doi: [10.1142/9789813229365_0006](https://doi.org/10.1142/9789813229365_0006).
- [28] R. Ramadoss, S. Lee, Y. C. Lee, V. M. Bright, and K. C. Gupta, "RF-MEMS capacitive switches fabricated using printed circuit processing techniques," *J. Microelectromech. Syst.*, vol. 15, no. 6, pp. 1595–1604, 2006, doi: [10.1109/JMEMS.2006.885854](https://doi.org/10.1109/JMEMS.2006.885854).
- [29] J. E. Rogers, R. Ramadoss, P. M. Ozmun, and R. N. Dean, "MEMS accelerometer fabricated using printed circuit processing techniques," in *Proc. IEEE Int. Symp. Ind. Electron.*, Jun. 2007, pp. 3250–3254, doi: [10.1109/ISIE.2007.4375135](https://doi.org/10.1109/ISIE.2007.4375135).
- [30] U. Dillner, E. Kessler, S. Poser, V. Baier, and J. Müller, "Low power consumption thermal gas-flow sensor based on thermopiles of highly effective thermoelectric materials," *Sens. Actuators A, Phys.*, vol. 60, nos. 1–3, pp. 1–4, 1997, doi: [10.1016/S0924-4247\(96\)01409-4](https://doi.org/10.1016/S0924-4247(96)01409-4).
- [31] J. S. Suehle, R. E. Cavicchi, M. Gaitan, and S. Semancik, "Tin oxide gas sensor fabricated using CMOS micro-hotplates and *in-situ* processing," *IEEE Electron Device Lett.*, vol. 14, no. 3, pp. 118–120, Mar. 1993, doi: [10.1109/55.215130](https://doi.org/10.1109/55.215130).
- [32] S. Z. Ali, F. Udrea, W. I. Milne, and J. W. Gardner, "Tungsten-based SOI microhotplates for smart gas sensors," *J. Microelectromech. Syst.*, vol. 17, no. 6, pp. 1408–1417, Dec. 2008, doi: [10.1109/JMEMS.2008.2007228](https://doi.org/10.1109/JMEMS.2008.2007228).
- [33] F. Udrea *et al.*, "Design and simulations of SOI CMOS micro-hotplate gas sensors," *Sens. Actuators, B, Chem.*, vol. 78, nos. 1–3, pp. 180–190, 2001, doi: [10.1016/S0925-4005\(01\)00810-3](https://doi.org/10.1016/S0925-4005(01)00810-3).
- [34] A. Petropoulos, D. N. Pagonis, and G. Kaltas, "Flexible PCB-MEMS flow sensor," *Proc. Eng.*, vol. 47, pp. 236–239, Jan. 2012, doi: [10.1016/j.proeng.2012.09.127](https://doi.org/10.1016/j.proeng.2012.09.127).
- [35] M. Leber, F. Solzbacher, and B. Baker, "Micro-electromechanical systems including printed circuit boards and pre-fabricated polymer films," U.S. Patent 061356 A2, Dec. 2020.
- [36] D. Beckel, D. Briand, A. Bieberle-Hütter, J. Courbat, N. F. de Rooij, and L. J. Gauckler, "Micro-hotplates—A platform for micro-solid oxide fuel cells," *J. Power Sources*, vol. 166, no. 1, pp. 143–148, Mar. 2007, doi: [10.1016/j.jpowsour.2006.12.072](https://doi.org/10.1016/j.jpowsour.2006.12.072).
- [37] H. Ji-Song, T. Kadokawa, K. Sato, and M. Shikida, "Fabrication of thermal-isolation structure for microheater elements applicable to finger-print sensors," *Sens. Actuators A, Phys.*, vol. 100, no. 1, pp. 114–122, 2002, doi: [10.1016/S0924-4247\(02\)00136-X](https://doi.org/10.1016/S0924-4247(02)00136-X).
- [38] K. A. A. Makinwa and J. H. Huijsing, "A smart wind sensor using thermal sigma-delta modulation techniques," *Sens. Actuators, A, Phys.*, vols. 97–98, pp. 15–20, Apr. 2002, doi: [10.1016/S0924-4247\(02\)00034-1](https://doi.org/10.1016/S0924-4247(02)00034-1).
- [39] T. J. Garrett, F. Solzbacher, and K. Shkurko, "Weather-detecting devices and related methods," U.S. Patent 0 326 456 A1, Oct. 15, 2020.
- [40] DuPont. *DuPont Kapton—Summary of Properties*. Accessed: Sep. 15, 2021. [Online]. Available: <https://www.dupont.com/content/dam/dupont/amer/us/en/products/ei-transformation/documents/EI-10142-Kapton-Summary-of-Properties.pdf>
- [41] J. Courbat, M. Barbieri, D. Briand, and N. F. de Rooij, "Reliability of micro-hotplates on polyimide foil," in *Proc. 16th Int. Solid-State Sens., Actuators Microsyst. Conf.*, Jun. 2011, pp. 338–341, doi: [10.1109/TRANSDUCERS.2011.5969465](https://doi.org/10.1109/TRANSDUCERS.2011.5969465).